Tropical Warm Pool Surface Heat Budgets and Temperature: Contrasts between 1997/98 El Niño and 1998/99 La Niña

SHU-HSIEN CHOU* AND MING-DAH CHOU*

Laboratory for Atmospheres, NASA Goddard Space Flight Center, Greenbelt, Maryland

PUI-KING CHAN

Science Systems and Applications, Inc., Lanham, Maryland

PO-HSIUNG LIN

National Taiwan University, Taipei, Taiwan

KUNG-HWA WANG

Central Weather Bureau, Taipei, Taiwan

(Manuscript received 17 February 2003, in final form 28 November 2003)

ABSTRACT

Seasonal to interannual variations of the net surface heating (F_{NET}) and its relationship to sea surface temperature tendency (dT_s/dt) in the tropical eastern Indian and western Pacific Oceans are studied for the period October 1997–September 2000. The surface heat fluxes are derived from the Special Sensor Microwave Imager and Japanese Geostationary Meteorological Satellite radiance measurements. It is found that the magnitude of solar heating is larger than that of evaporative cooling, but the spatial variation of the latter is significantly larger than the former. As a result, the spatial patterns of the seasonal and interannual variability of F_{NET} are dominated by the variability of evaporative cooling. Seasonal variations of F_{NET} and dT_s/dt are significantly correlated, except for the equatorial western Pacific. The high correlation is augmented by the high negative correlation between solar heating and evaporative cooling.

The change of F_{NET} between the 1997/98 El Niño and 1998/99 La Niña is significantly larger in the tropical eastern Indian Ocean than that in the tropical western Pacific. For the former region, reduced evaporative cooling arising from weakened winds during El Niño is generally associated with enhanced solar heating due to reduced cloudiness, leading to enhanced interannual variability of F_{NET}. For the latter region, reduced evaporative cooling due to weakened winds is generally associated with reduced solar heating arising from increased cloudiness, and vice versa. Consequently, the interannual variability of F_{NET} is reduced. The correlation between interannual variations of F_{NET} and dT_s/dt is weak in the tropical western Pacific and eastern Indian Oceans, indicating the importance of ocean dynamics in affecting the interannual SST variation.

1. Introduction

The warm pool of the tropical Indian and western Pacific Oceans is a climatically important region, characterized by the warmest sea surface temperature (SST), frequent heavy rainfall, strong atmospheric heating, and weak mean winds with highly intermittent westerly wind bursts. The heating drives the global climate and plays a key role in the El Niño–Southern Oscillation (ENSO) and the Asian–Australian monsoon (Webster et al. 1998). Small changes in the SST of the Pacific warm pool associated with eastward shift of the warm pool during ENSO events have been shown to affect the global climate (Palmer and Mansfield 1984). Thus, the Tropical Ocean Global Atmosphere (TOGA) Coupled Ocean–Atmosphere Response Experiment (COARE) was conducted with the aim to better understand various physical processes responsible for the SST variation in the western Pacific warm pool (e.g., Anderson et al. 1996; Sui et al. 1997; Godfrey et al. 1998; Chou et al. 2000).

During 1997/98, one of the strongest El Niño warm events took place in the tropical Pacific Ocean and a

* Current affiliation: Department of Atmospheric Sciences, National Taiwan University, Taipei, Taiwan.

Corresponding author address: Dr. Shu-Hsien Chou, Department of Atmospheric Sciences, National Taiwan University, 1, Section 4, Roosevelt Road, Taipei 106, Taiwan.
E-mail: shchou@atmos1.as.ntu.edu.tw

record-breaking SST warming occurred in the entire Indian Ocean (Yu and Reinecker 2000; Bell et al. 1999). In addition, during July–December 1997, the SST was observed to have a negative anomaly in the eastern equatorial Indian Ocean and a positive anomaly in the western equatorial Indian Ocean, which were referred to as the Indian Ocean dipole mode. The SST anomalies were large enough to reverse the climatological equatorial SST gradient. The strong 1997/98 El Niño, which was followed by the moderate 1998–2000 La Niña, had rapid onset and decay (McPhaden 1999; Bell et al. 1999, 2000). The unusual nature of both events has motivated many studies to investigate the physical processes responsible for the events, the relation of ENSO and Indian Ocean climate system, and various ENSO theories (e.g., Webster et al. 1999; Saji et al. 1999; Yu and Rienecker 2000; Wang and McPhaden 2001 and references therein).

To understand the interannual variations of SST, the information on the seasonal to interannual variability of the surface heat budgets and the correlation of surface heating with SST tendency in the tropical warm pool is particularly important. Because reliable information on the annual mean and seasonal cycle can help improve the creditability of the information on the interannual changes, analysis of the annual mean and seasonal cycle is essential. In this study, we investigate the seasonal to interannual variations of the surface heat budgets and their relationships to SST tendency over the tropical eastern Indian and western Pacific Oceans (30°S–30°N, 90°E–170°W) during the 3-yr period, October 1997–September 2000, using the Goddard Satellite-Retrieved Surface Radiation Budget (GSSRB; Chou et al. 2001) and Goddard Satellite-Based Surface Turbulent Fluxes, version 2 (GSSTF2; Chou et al. 2003). During this period, there were the strong 1997/98 El Niño and the moderate 1998/99 La Niña (Bell et al. 1999, 2000).

Surface measurements of the radiative and turbulent fluxes are scarce in both space and time. The Comprehensive Ocean–Atmosphere Data Set (COADS) has collected the most complete surface marine observations since 1854, mainly from merchant ships (Woodruff et al. 1993). However, the air–sea fluxes and input variables based on COADS have serious spatial and temporal sampling problems plus measurement uncertainty (e.g., da Silva et al. 1994; Josey et al. 1999; Wang and McPhaden 2001).

Several efforts are underway to prepare datasets of ocean surface turbulent fluxes from satellite observations using bulk flux models (Curry et al. 2003 and references therein). The Special Sensor Microwave Imager (SSM/I) on board a series of the Defense Meteorological Satellite Program (DMSP) spacecraft has provided global radiance measurements for sensing the atmosphere and the surface. A number of techniques have been developed to derive the turbulent fluxes using parameters such as the surface air humidity and winds inferred from the SSM/I radiances (e.g., Chou et al. 1997, 2003; Schulz et al. 1997; Curry et al. 2003; Kubota et al. 2002). Chou et al. (2003) derived the GSSTF2 over global oceans from SSM/I radiance measurements, covering a 13.5-yr period (July 1987–December 2000). The GSSTF2 has a spatial resolution of 1° latitude × 1° longitude and a temporal resolution of 1 day.

Surface radiation has been either computed using satellite-retrieved cloud and other atmospheric parameters or directly derived from satellite radiance measurements. The National Aeronautics and Space Administration (NASA) Langley global surface radiation datasets consist of monthly shortwave (SW) and longwave (LW) fluxes for the 8-yr period (July 1983–June 1991). These datasets are computed using fast radiation parameterizations and satellite data from the International Satellite Cloud Climatology Project (ISCCP) and the Earth Radiation Budget Experiment (ERBE) (Gupta et al. 1999). The NASA Goddard Institute for Space Studies (GISS) surface radiation datasets are computed using a detailed radiative transfer model (Zhang et al. 1995). Cloud data are taken from the ISCCP data archive. Currently, the GISS monthly surface radiation datasets cover a period of 18 years (1983–2000). The NASA GSSRB is retrieved empirically from the Japanese *Geostationary Meteorological Satellite 5* (*GMS-5*) radiance measurements (Chou et al. 2001). The surface SW and LW radiation is first retrieved hourly and then averaged to daily values. The GSSRB covers the domain 40°S–40°N, 90°E–170°W and the period from October 1997 to December 2000. The spatial resolution is 0.5° latitude × 0.5° longitude and the temporal resolution is 1 day.

In section 2, we briefly describe the data used, as well as the methods for deriving the surface fluxes and the retrieval accuracy. Section 3 presents the spatial distributions of annual-mean surface heat fluxes and some relevant parameters used for deriving the surface fluxes. Section 4 discusses the seasonal variation of surface heat fluxes and the SST tendency. Section 5 compares the surface heat fluxes, SST, SST tendency, outgoing longwave radiation (OLR), surface wind speed, and zonal wind stress between the 1997/98 El Niño and the 1998/99 La Niña. Concluding remarks are given in section 6.

2. Data sources, retrieval of surface fluxes, and collocation validation

a. Data sources

The basic data used for heat budget analysis are 1° latitude × 1° longitude daily mean surface radiative and turbulent fluxes (momentum, latent heat, and sensible heat), SST, surface wind speed (U_{10m}), and sea–air humidity difference ($Q_s - Q_{10m}$), and monthly mean OLR, during the 3-yr period of October 1997–September 2000. Radiative fluxes are taken from GSSRB (Chou et al. 2001), and turbulent fluxes, U_{10m}, ($Q_s - Q_{10m}$), and SST are taken from GSSTF2 (Chou et al. 2003). The OLR inferred from the National Oceanic and Atmo-

TABLE 1. The periods and locations of five tropical field experiments conducted by the NOAA/ETL research ships.

Experiments	Periods	Locations
ASTEX	6–28 Jun 1992	30°N, 36°W
COARE	11 Nov 1992–16 Feb 1993	1.7°S, 156°E
JASMINE	4–31 May 1999	5°S–13°N, 88°–98°E
KWAJEX	28 Jul–10 Sep 1999	9°N, 167°E
NAURU99	15 Jun–18 Jul 1999	12°S, 130°E to 8°N, 167°E

spheric Administration (NOAA) Advanced Very High Resolution Radiometer (Gruber and Winston 1978) is used as proxy for deep convection and cloudiness.

Monthly mean radiative and turbulent fluxes are derived from daily mean values. For those days with missing data, the heat fluxes are interpolated spatially from those of the neighboring eight grid points and temporally from those of the neighboring days. The spatial and temporal interpolations are alternately applied to the entire heat flux datasets, with three times of interpolation for space and twice for time. The amount of missing data after interpolation is ~1%–3% over most of the domain, except for two small areas in the Bay of Bengal and South China Sea. The amount of missing data after interpolation is ~3%–20% in the Bay of Bengal (10°–22°N, 90°–100°E) and ~3%–10% over the South China Sea area (10°–23°N, 110°–130°E). The monthly means are derived only from those days when all four components of the heat flux are available.

To validate the GSSTF2 turbulent fluxes and input parameters, hourly measurements of surface meteorology and turbulent fluxes of five field experiments, conducted by the NOAA/Environmental Technology Laboratory (ETL) research ships, over the tropical oceans during 1992–99 are used (Fairall et al. 2003). Table 1 shows the periods and locations of the five tropical experiments: the Atlantic Stratocumulus Transition Experiment (ASTEX), COARE (Fairall et al. 1996), the Joint Air–Sea Monsoon Interaction Experiment (JASMINE: Webster et al. 2002), the Kwajalein Experiment (KWAJEX), and the Nauru 1999 Experiment (NAURU99). These experiments provide hourly latent and sensible heat fluxes derived with the eddy correlation method. They also provide hourly wind stress determined with the inertial-dissipation (ID) method. The wind stress derived with the ID method is more accurate than that derived with the eddy correlation method using ship measurements (Fairall et al. 1996).

b. Derivation and validation of GSSRB surface radiation

A number of studies have shown that SW radiation at the surface and the top of the atmosphere are highly correlated, and the surface SW radiation can be directly derived from satellite radiation measurements (e.g., Li and Leighton 1993; Pinker et al. 1995). Chou et al. (2001) retrieved the surface SW radiation empirically

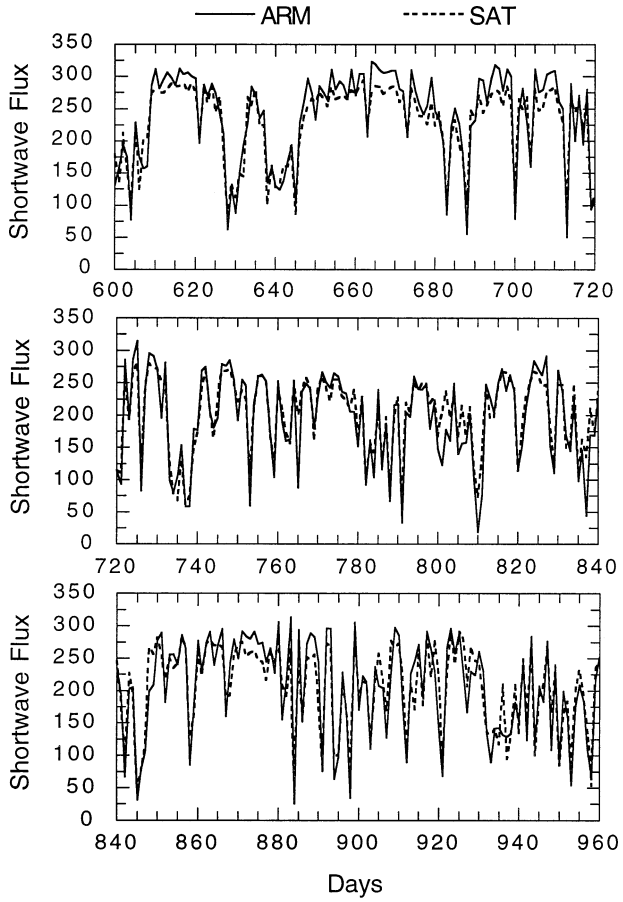

FIG. 1. Daily variations of downward surface SW flux measured at the ARM Manus site (2.06°S, 147.43°E) and retrieved from *GMS-5* albedo measurements. Comparison is shown only for the period Dec 1999–Dec 2000. Units of flux are W m^{-2}.

from the solar zenith angle and the albedo measured in the visible channel of the *GMS-5*. The surface radiation was originally retrieved hourly with a spatial resolution of 25 km and subsequently averaged to daily values with a spatial resolution of 0.5° latitude × 0.5° longitude. It is further degraded to a resolution of 1° latitude × 1° longitude in this study. The surface radiation dataset, GSSRB, covers the domain 40°S–40°N, 90°E–170°W and the period October 1997–December 2000. The retrieved surface radiation has been validated against the observations at the Department of Energy's Atmospheric Radiation Measurement (ARM) site on Manus Island (2.06°S, 147.43°E) (Mather et al. 1998). Figure 1 shows daily variations of the observed (solid curve) and retrieved (dashed curve) downward SW radiation at the Manus site during the 13-month period of December 1999–December 2000. It can be seen that the retrieved SW radiation is in good agreement with the measured SW radiation. Averaged over the entire GSSRB period (October 1997–December 2000), the retrieved daily mean downward surface SW flux has a positive bias of 6.7 W m^{-2} and a standard deviation

(SD) error of 28.4 W m^{-2}. Assuming that errors of the retrieved daily radiation are independent, the SD error of the monthly mean SW radiation reduces to 5.2 W m^{-1}.

The surface LW radiation depends strongly on the temperature and humidity of the surface boundary layer and only moderately relates to the radiation at the top of the atmosphere. The GSSRB surface LW radiation is derived from the surface temperature, atmospheric column water vapor amount, and the brightness temperature measured in the 11-μm channel of the *GMS-5*. The net surface LW radiation varies within a small range and the error in the retrievals is small (not shown). Compared to the surface measurements at the ARM Manus site, the daily downward surface LW radiation of GSSRB has a bias of +2.3 W m^{-2} and a SD error of 6.6 W m^{-2}. Assuming that errors of the retrieved daily radiation are independent, the SD error of the monthly mean LW radiation reduces to 1.2 W m^{-2}. The biases of the SW and LW radiative fluxes have been subtracted from the satellite retrievals in this study.

c. Derivation and validation of GSSTF2 retrievals

The GSSTF2 covers global oceans and the period July 1987–December 2000. Chou et al. (2003) discussed and validated the GSSTF2 bulk flux model, daily turbulent fluxes, and daily input parameters using ship measurements of the 10 field experiments conducted by the NOAA/ETL. Briefly, the GSSTF2 flux model is a bulk aerodynamics algorithm based on the Monin–Obukhov similarity theory including the salinity and cool-skin effects. The daily mean input parameters for turbulent flux calculations include SSM/I 10-m wind speed (U_{10m}) of Wentz (1997), the 10-m specific humidity (Q_{10m}), which is derived from the precipitable water of the entire atmospheric column and the 500-m layer near the surface (Chou et al. 1997). The input parameters also include the 2-m air temperature (T_{2m}) and SST of the National Centers for Environmental Prediction–National Center for Atmospheric Research (NCEP–NCAR) reanalysis (Kalney et al. 1996). The directions of wind stress are taken from those of the surface winds, which are derived from a blend of the SSM/I U_{10m}, surface wind vectors from ships, buoys, and the NCEP–NCAR reanalysis following the method of Atlas et al. (1996).

Table 2 compares daily turbulent fluxes and input parameters between GSSTF2 and the five tropical field experiments shown in Table 1. Using the GSSTF2 flux model, the GSSTF2 daily wind speed (U), specific humidity (Q_a), and temperature (T_a) of the surface air are adjusted to the measurement heights of the ships (~14–21 m) for proper validation. Compared to 134 daily turbulent fluxes of these five experiments, latent heat flux (F_{LH}) of GSSTF2 has a negative bias of −2.6 W m^{-2}, a SD error of 29.7 W m^{-2}, and a correlation of 0.80. Sensible heat flux (F_{SH}) has a positive bias of 7.0 W m^{-2}, a SD error of 6.2 W m^{-2}, and a correlation of 0.45. Daily wind stress has a positive bias of 0.0053 N m^{-2}, a SD error of 0.0193 N m^{-2}, and a correlation of 0.81. The positive bias of the F_{SH} is mainly due to the negative bias (−0.83°C) of surface air temperature of the NCEP–NCAR reanalysis in the tropical oceans. Note that sources of discrepancies in turbulent fluxes and input parameters between satellite retrievals and ship observations include the spatial–temporal mismatch between GSSTF2 and ships, as well as the errors in the input parameters and fluxes of both GSSTF2 and ship observations. The collocated daily variables of GSSTF2 are computed from two or three satellite observations averaged over a 1° latitude × 1° longitude area that encloses the ship locations, while those of the ships are computed from at least two hourly measurements over a much smaller area. Assuming daily retrieval errors are independent, the SD errors of the monthly mean F_{LH}, F_{SH}, and wind stress reduce to 5.4 W m^{-2}, 1.1 W m^{-2}, and 0.0035 N m^{-2}, respectively.

TABLE 2. Comparison of daily latent heat fluxes (F_{LH}), sensible heat fluxes (F_{SH}), wind stress, surface wind speed (U), surface air humidity (Q_a), surface air temperature (T_a), and SST of GSSTF2 with those of ship measurements during five tropical field experiments. The mean is the ship-observed values averaged over 134 days of collocation. Positive bias indicates larger GSSTF2, SD error is std dev of differences, and r is correlation coefficient.

				SD error		
Variable	Unit	Mean	Bias	Daily	Monthly	r
F_{LH}	W m^{-2}	93.0	−2.6	29.7	5.4	0.80
F_{SH}	W m^{-2}	5.5	7.0	6.2	1.1	0.45
Stress	10^{-3} N m^{-2}	32.7	5.3	19.3	3.5	0.81
U	m s^{-1}	4.5	0.34	1.12	0.20	0.85
Q_a	g kg^{-1}	17.8	1.01	1.10	0.20	0.85
T_a	°C	27.4	−0.83	0.73	0.13	0.94
SST	°C	28.5	−0.01	0.31	0.06	0.99

3. Annual mean surface heat budgets

a. Surface heat budgets

In this section we present the spatial distributions of surface heat budgets and relevant parameters over the tropical eastern Indian and western Pacific Oceans (30°S–30°N, 90°E–170°W) for the 3-yr (October 1997–September 2000) mean condition. The period October 1997–May 1998 is part of the 1997/1998 El Niño, while June 1998–September 2000 is part of the 1998–2000 La Niña (Bell et al. 1999, 2000). The mean conditions for the 3-yr period of October 1997–September 2000 are likely close to the long-term means. The downward net heat flux F_{NET} at the surface is given by

$$F_{NET} = F_{SW} - (F_{LW} + F_{LH} + F_{SH}), \quad (1)$$

where F_{SW} is the downward net shortwave flux (solar heating), F_{LW} is the upward net longwave flux (IR cooling), F_{LH} is the upward latent heat flux (evaporative cooling), and F_{SH} is the upward sensible heat flux. The spatial distributions of the 3-yr mean F_{SW}, F_{LW}, F_{LH},

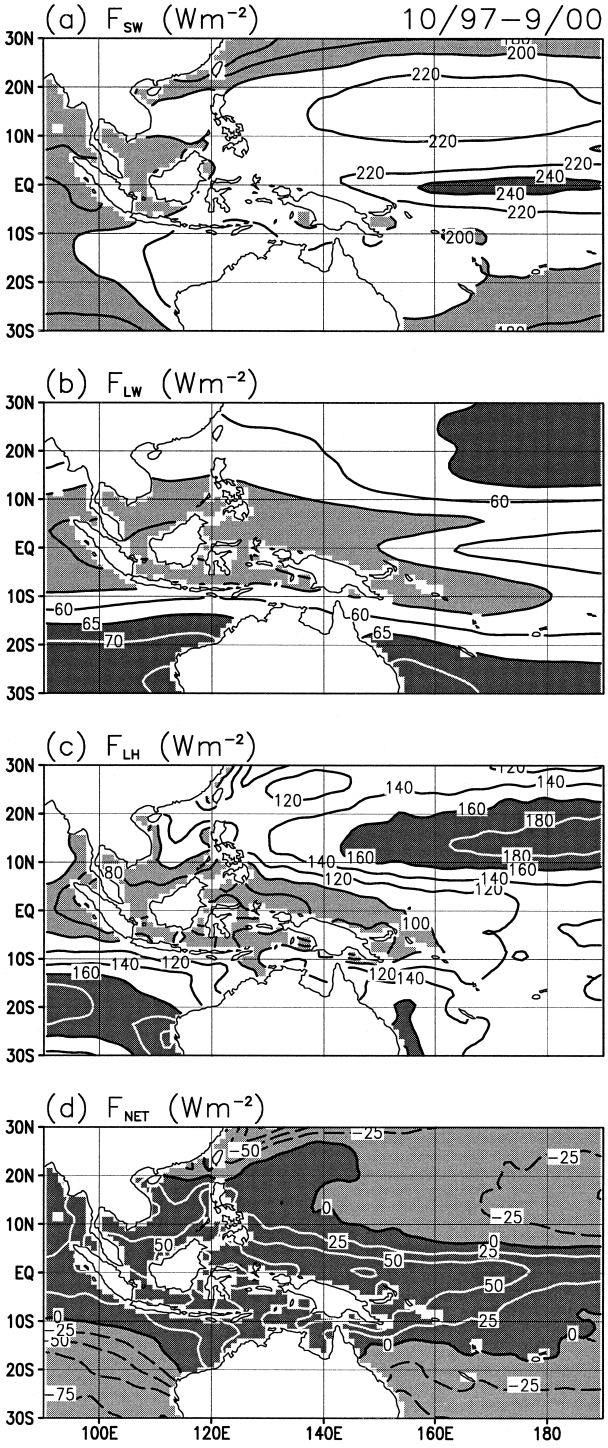

FIG. 2. Surface (a) solar heating, (b) IR cooling, (c) evaporative cooling, and (d) net heating, averaged over the 3-yr period Oct 1997–Sep 2000. Regions of large values are marked with dark shading, and regions of small values are marked with light shading.

and F_{NET} are shown in Fig. 2. The F_{SH} is generally very small (~5–15 W m^{-2}) and is not shown. It can be seen from Fig. 2 that ranges of the 3-yr mean F_{SW}, F_{LW}, and F_{LH} are ~180–240, 50–70, and 80–190 W m^{-2}, respectively. Among the heat flux components, F_{SW} has the largest magnitude, and F_{LH} has the largest spatial variation. The spatial variation of F_{LW} is very small. As a result, the spatial variation of F_{NET} is dominated by F_{LH}. For the 3-yr mean condition within ~10°–15° of the equator, the oceans gain heat up to ~50–75 W m^{-2}, due to the large solar heating and small evaporative cooling. Poleward of this region, the heat loss by the ocean increases with latitudes primarily due to an increase in evaporative cooling.

b. Relationships of surface heat fluxes to relevant parameters

The spatial distributions of the parameters relevant to the surface fluxes averaged over the 3-yr period are shown in Fig. 3. The deep convective cloudiness, as indicated by OLR $<$ 240 W m^{-2}, occurs in the Maritime Continent, the intertropical convergence zone (ITCZ, centered at ~7°N), and the southern Pacific convergence zone (SPCZ, centered at ~10°S) (Fig. 3a). Generally, the spatial distribution of annual-mean solar heating (Fig. 2a) resembles only slightly that of clouds. It reflects the fact that solar heating depends not only on clouds but also on the seasonal and latitudinal variations of insolation at the top of the atmosphere. The SST contour of 29°C encompasses a large equatorial region west of the date line (Fig. 3b). The longwave cooling depends on clouds, SST, and the temperature and humidity of the atmospheric boundary layer. Although the range of LW cooling is small (Fig. 2b), its spatial distribution resembles closely that of clouds (or OLR). Figure 3c shows that the sea–air humidity difference ($Q_s - Q_{10m}$) is large, ~5–6 g kg^{-1} but the spatial variation is small. On the other hand, the spatial variation of the annual-mean surface (10 m) wind speed is large, which varies by a factor $>$2 from 4 to 9 m s^{-1} (Fig. 3d). The surface wind speed has a minimum in the equatorial convergence region and a maximum in the trade wind regions. The spatial distribution of the evaporative cooling (Fig. 2c) is determined primarily by wind speed and secondarily by $Q_s - Q_{10m}$. The minimum evaporative cooling of 80–100 W m^{-2} in the Maritime Continent coincides with the minimum wind speed (4–5 m s^{-1}) and $Q_s - Q_{10m}$ (~5 g kg^{-1}). The maximum evaporative cooling of ~180 W m^{-2} occurs in the trade wind regimes where the wind speed (8–9 m s^{-1}) and $Q_s - Q_{10m}$ (~6 g kg^{-1}) are both large.

c. Comparison with other studies

We have compared the spatial distributions of the 3-yr mean surface turbulent heat fluxes with those of the 13-yr mean (1988–2000) fluxes from the GSSTF2

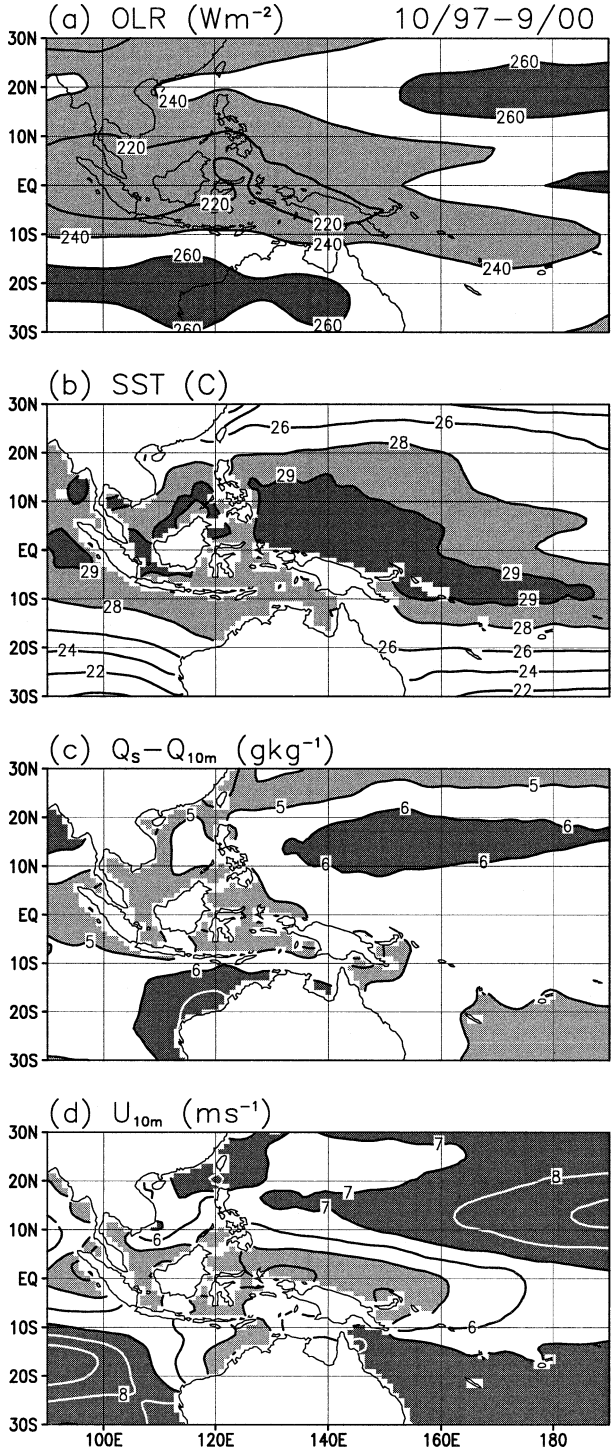

FIG. 3. (a) OLR, (b) SST, (c) sea–air humidity difference, and (d) 10-m wind speed, averaged over the 3-yr period Oct 1997–Sep 2000. Regions of large values are marked with dark shading, and regions of small values are marked with light shading, except for (b).

(Chou et al. 2003). It is found that the results are essentially the same for the region under study, except that the 3-yr mean F_{LH} over the trade wind regions is larger than the 13-yr mean by ~5–20 W m^{-2}. This is due to a slightly higher wind speed (by ~0.5 m s^{-1}) and $Q_s - Q_{10m}$ (by ~0.5 g kg^{-1}) for the 3-yr mean. Kubota et al. (2002) constructed the Japanese Ocean Flux datasets with Use of Remote Sensing Observation (J-OFURO). Compared to Fig. 2, the J-OFURO F_{SW} is larger by up to ~20 W m^{-2}. The F_{LH} is smaller by ~20–40 W m^{-2} in the equatorial region but is larger by ~20 W m^{-2} in the subtropics. For the F_{LW} it is smaller by ~10–15 W m^{-2} in the equatorial area but is larger by 5–15 W m^{-2} in the subtropics. As a result of these differences, the meridional gradient of the J-OFURO F_{NET} is greater than that of our F_{NET} due to a larger surface heating in the equatorial warm pool region (~15–30 W m^{-2}) and a larger cooling in the trade wind belts (~10–15 W m^{-2}). The discrepancy of surface heat budgets between this study and J-OFURO is partly due to the difference in time periods of studies and partly due to the difference in retrieval techniques (see Chou et al. 2001; Chou et al. 2003; Kubota et al. 2002).

The spatial distributions shown in Fig. 2 are also similar to those of Oberhuber (1988), which were derived from COADS covering the period 1950–79 with the data primarily taken from ship observations. Compared to Oberhuber (1988), however, our F_{SW} is larger by ~25–40 W m^{-2}, F_{LW} is larger by ~10 W m^{-2}, F_{LH} is larger by up to ~25 W m^{-2} in the trade wind regions, and F_{SH} is larger by ~5 W m^{-2}. Generally, our F_{NET} is larger than that of Oberhuber (1988) by up to ~30 W m^{-2} in the equatorial region, but smaller by a maximum of ~30 W m^{-2} in the south Indian Ocean trade wind region. Wang and McPhaden (2001) examined the surface heating at four locations along the equator using the Tropical Atmosphere Ocean (TAO) buoy observations. Two of the locations (165°E and 170°W) are in the western Pacific domain. From the curves shown in their Figs. 4c and 4d, we estimated that the net surface heating is ~75 W m^{-2} at 165°E and ~95 W m^{-2} at 170°W during the period August 1997–July 1999. From Fig. 2d, our estimation of the net surface heating is in good agreement at 165°E (70 W m^{-2}) but is significantly smaller at 170°W (35 W m^{-2}).

Gent (1991) examined the annual-mean surface heat budget of the TOGA COARE domain in a reduced-gravity primitive equation model of the upper equatorial ocean with forcing of parameterized monthly mean wind stresses and surface net heat fluxes. He found that net surface heating increased eastward toward lower SST in the Pacific warm pool, increasing from ~5 W m^{-2} at 140°E to ~50 W m^{-2} at 180° near the equator. Based on the model-derived F_{NET}, he suggested that the annual mean F_{NET} was between 0 and 20 W m^{-2} in the region 10°S–10°N, 140°E–180°. Moisan and Niiler (1998) estimated the heat budget of the North Pacific Ocean for the period 1950–90 by balancing the net surface heat

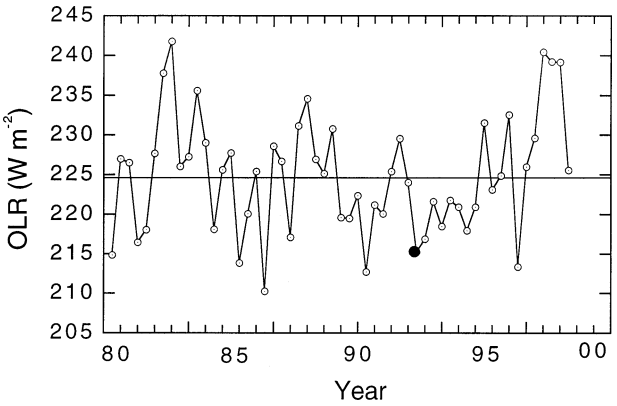

FIG. 4. Outgoing longwave radiation averaged over the COARE region. Each data point represents a 4-month mean. The first data point corresponds to the mean of the period Nov 1980–Feb 1981. The OLR of the COARE IOP (Nov 1992–Feb 1993) is marked with a solid circle. The horizontal line represents the mean OLR of the 18-yr period Nov 1980–Feb 1999.

flux with the heat storage rate of the ocean upper layer with the assumption of no heat transfer at the bottom of the layer. They found that the net surface heating is weak in the equatorial region, with a cooling in the TOGA COARE domain and a weak heating confined only to a narrow band west of 140°E. The results of Gent (1991) and Moisan and Niiler (1998) are different from that of our study, the studies of Kubota et al. (2002), and Oberhuber (1988) in that strong net surface heating is found across the equatorial band between 10°S and 10°N.

The 3-yr mean net surface heating shown in Fig. 2d is also significantly larger than that of the TOGA COARE Intensive Observing Period (IOP) from November 1992 to February 1993 (e.g., Weller and Anderson 1996; Chou et al. 2000). The OLR taken from the NOAA data archive shows that the entire COARE region (10°S–10°N, 135°E–175°E) is covered with high cloudiness (OLR $<$ 240 W m^{-2}) during the COARE IOP. Table 3 shows that the mean OLR during the COARE IOP averaged over the COARE domain is 215 W m^{-2}, which is much less than that of the same 4-month periods from 1997 to 2000, as well as the 3-yr mean of 1997–2000. Because of the high cloudiness during the COARE IOP, the surface SW radiation is much reduced as compared to the other periods shown in the table. The net surface heating during the COARE IOP is only 7 W m^{-2}. To further demonstrate that the equatorial western Pacific is abnormally cloudy during the COARE IOP, we show, in Fig. 4, time series of the 4-month mean OLR averaged over the COARE region for the 18-yr period from November 1980 to February 1999. The COARE IOP mean (215 W m^{-2}) is significantly less than the long-term mean (225 W m^{-2}). Among the 55 4-month periods, there are only 5 periods with smaller OLR than what is inferred for the COARE IOP. It further indicates that the equatorial western Pacific is unusually cloudy during the COARE IOP.

TABLE 3. Comparison of OLR and surface heat budgets of the Pacific warm pool (10°S–10°N, 135°–175°E) among the 4-month (Nov–Feb) periods of 1992/93, 1997/98, 1998/99, and 1999/2000, as well as the 3-yr period of Oct 1997–Sep 2000. Units are W m^{-2}.

Parameter	Nov–Feb				3 yr
	1992/93	1997/98	1998/99	1999/2000	1997–2000
OLR	215	240	226	228	232
F_{SW}	193	221	212	218	216
F_{LW}	53	57	55	56	55
F_{LH}	113	127	125	119	112
F_{SH}	20	11	9	10	10
F_{NET}	7	26	23	33	40

4. Seasonal variations of net surface heating and SST tendency

Seasonal variations of F_{NET} and SST tendency (dT_s/dt) over the tropical eastern Indian and western Pacific Oceans are investigated for the boreal winter [December–February (DJF)], spring [March–May (MAM)], summer [June–August (JJA)], and fall [September–November (SON)] of the 3-yr period from October 1997 to September 2000. Figure 5 shows the spatial distributions of the deviation of seasonal mean F_{NET} from the 3-yr mean. The ITCZ follows the sun to the summer hemisphere, and the trade winds are stronger in the winter hemisphere than in the summer hemisphere. The weak solar heating and the strong evaporative cooling cause a strong wintertime cooling of the ocean. In contrast, the weak evaporative cooling and strong solar heating cause a strong summertime heating. The contrast between summertime heating and wintertime cooling is very large, ~150 W m^{-2} at 20° latitude in both hemispheres (Figs. 5a and 5c). The F_{NET} increases during spring and summer in both hemispheres but decreases during fall and winter, except for the equatorial region. The magnitude of the seasonal deviation of F_{NET} from the annual mean increases poleward as the seasonal variations of both F_{SW} and F_{LH} increase poleward. The seasonal variation of F_{NET} is larger in the Northern Hemisphere than in the Southern Hemisphere, mainly due to a larger seasonal variation of F_{LH} in the Northern Hemisphere.

Figure 6 shows the seasonal dT_s/dt averaged over the same 3-yr period. Consistent with the seasonal variation of F_{NET} the SST increases during spring and summer of both hemispheres but decreases during fall and winter, except for the equatorial region. The seasonal variation of dT_s/dt is larger in the Northern Hemisphere than in the Southern Hemisphere, which is also consistent with the seasonal variation of F_{NET} (Fig. 5). The magnitude of dT_s/dt increases poleward as the seasonal variation of SST increases poleward.

Figure 7 shows the correlation coefficient r of month-

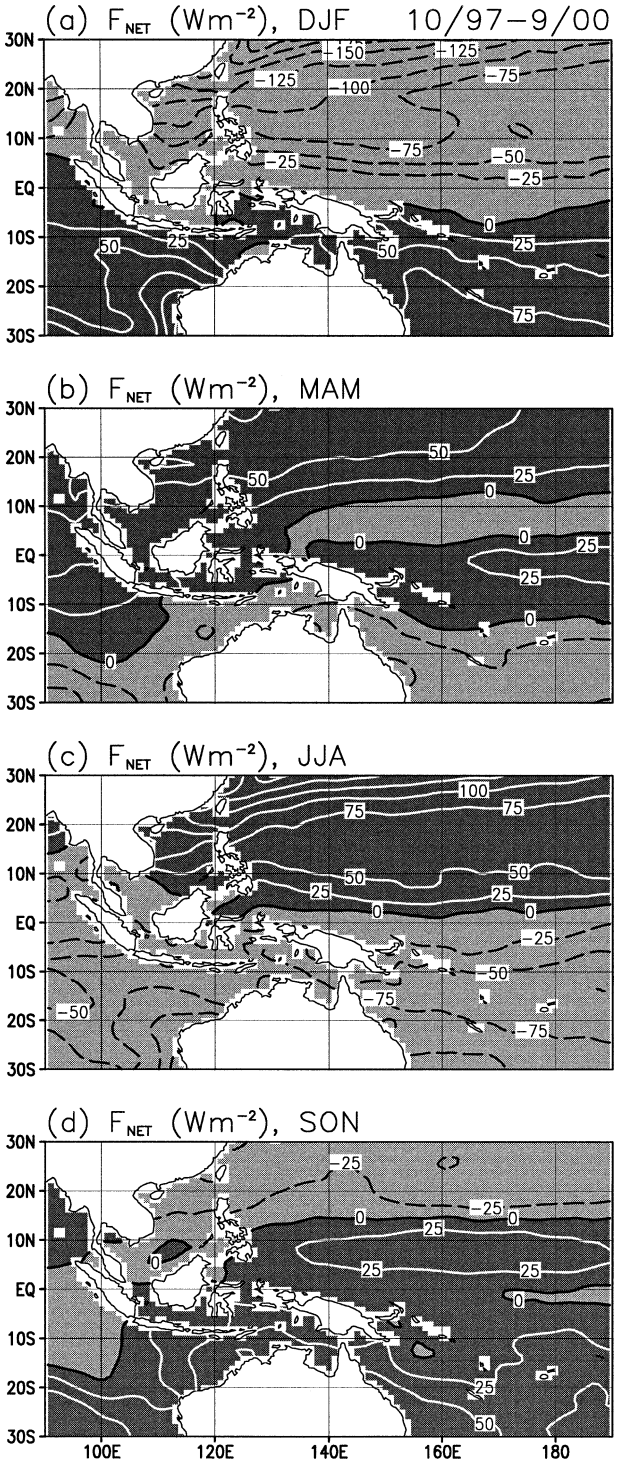

FIG. 5. Deviations of seasonal mean net surface heating from the 3-yr mean for the boreal (a) winter (DJF), (b) spring (MAM), (c) summer (JJA), and (d) fall (SON) of Oct 1997–Sep 2000. Positive values are marked with dark shading, and negative values are marked with light shading.

ly dT_s/dt and F_{NET}, F_{SW}, and $-F_{LH}$ for the 3-yr period. The regions where the correlation is significant at a 95% level are shaded in the figure. To determine the significance of the correlation, the standard deviation of the correlation coefficient, SD, is derived following the approach of Lau and Chan (1983). The correlation is considered significant if $r > 2$ SD, which has a 95% confidence level. It is found that regions of $r > 2$ SD generally coincide with regions of $r > 0.5$–0.6 for all three cases of correlation shown in the figure. Figure 7a shows that the correlation between monthly dT_s/dt and F_{NET} increases poleward and is generally very high, $r \sim 0.8$–0.9 poleward of 15°–20° latitude. The correlation is generally lower, $r \sim 0.4$–0.6, in the western Pacific within $\sim 10°$ of the equator. Thus, the seasonal variations of dT_s/dt and F_{NET} are significantly correlated at a confidence level of ~95% except for some small areas in the equatorial western Pacific. The correlation pattern shown in Fig. 7a is consistent with the patterns of the seasonal variations of F_{NET} and dT_s/dt shown in Figs. 5 and 6. For the north Indian Ocean, Loschnigg and Webster (2000) found that the seasonal variation of ocean heat storage was nearly balanced by that of the oceanic heat transport through the equator and that the correlation between seasonal variations of net surface heating and ocean heat storage was poor. Our results do not support their conclusion in the northeastern Indian Ocean, as the correlation (>0.6) is significant there.

Figure 7b shows that the correlation between monthly dT_s/dt and F_{SW} increases poleward and is generally very high, ~0.8–0.9 poleward of 10° latitude, but the correlation within ~10° of the equator is weak, ranging from −0.2 to 0.6. Thus, the seasonal variations of dT_s/dt and F_{SW} are significantly correlated at a confidence level of ~95% except for the equatorial region. The correlation between monthly dT_s/dt and $-F_{LH}$ is shown in Fig. 7c. Comparing Figs. 7b and 7c, it can be seen that dT_s/dt has a higher correlation with F_{SW} than $-F_{LH}$ except for the western equatorial Pacific ~5°S–5°N, 150°E–170°W. In the equatorial regions, the weak correlation of dT_s/dt with F_{SW} and F_{NET} is likely due to a large SW radiation penetration through the shallow ocean mixed layer associated with weak winds, together with the small seasonal variations of F_{SW} and F_{NET}. The importance of the SW radiation penetration in affecting the SST variation is one of the major findings from TOGA COARE (e.g., Anderson et al. 1996; Sui et al. 1997; Godfrey et al. 1998; Chou et al. 2000). Note that, when the mixed layer reaches the thermocline during intermittent strong westerly wind bursts, the entrainment of cold water from the thermocline can also decrease the correlation of dT_s/dt with F_{SW} and F_{NET}.

5. Comparison between the 1997/98 El Niño and 1998/99 La Niña

The central and eastern equatorial Pacific warms significantly during May 1997–May 1998, corresponding

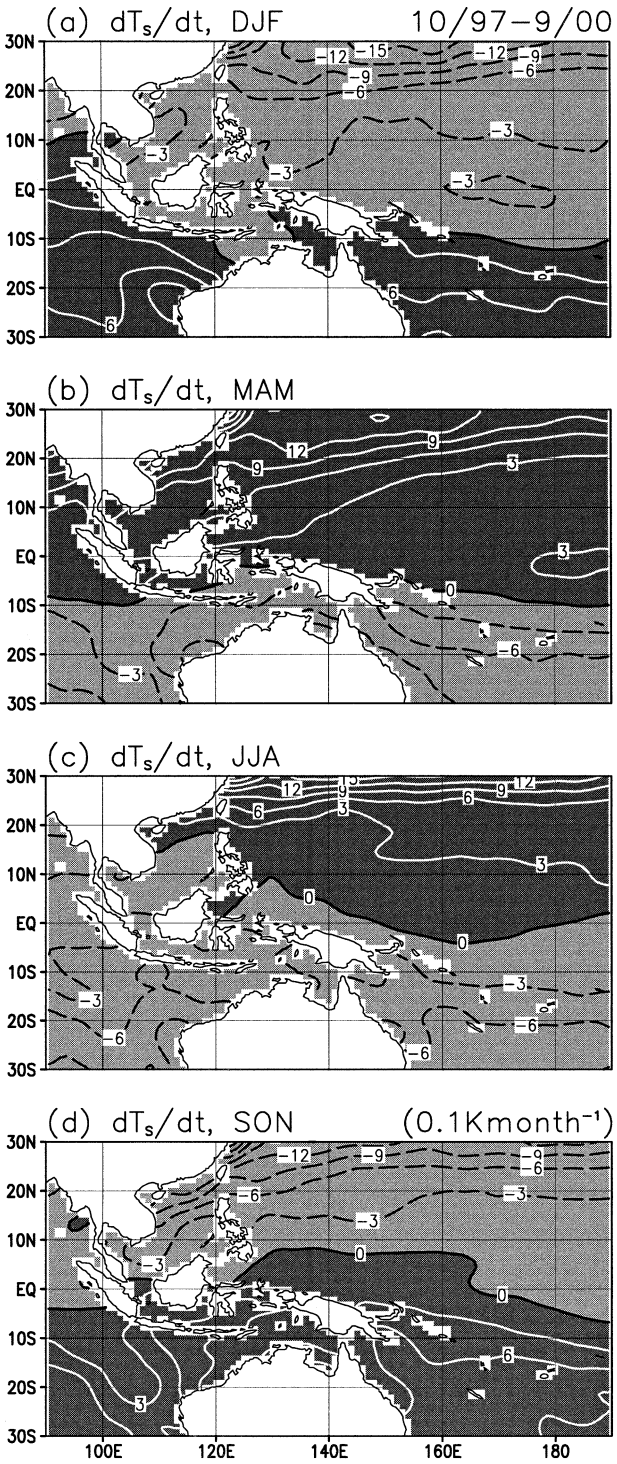

FIG. 6. As in Fig. 5 except for the seasonal-mean SST tendency. Units are 0.1 K month^{-1}.

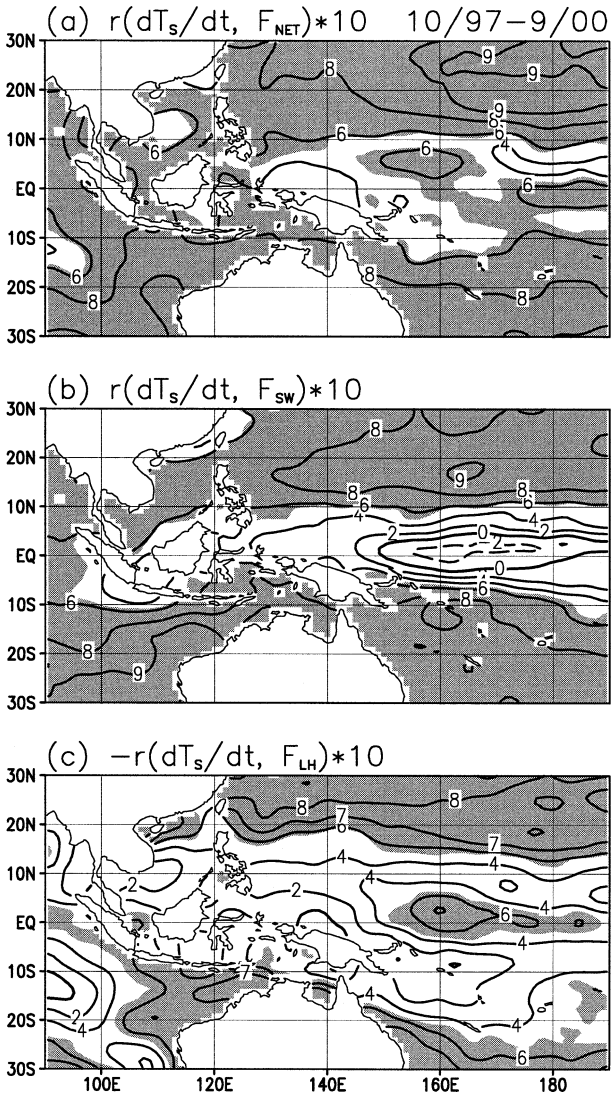

FIG. 7. Correlation coefficients of monthly SST tendency and monthly (a) net surface heating, (b) solar heating, and (c) evaporative heating for the 3-yr period Oct 1997–Sep 2000. Shaded areas indicate correlation significant at the 95% level.

to a strong El Niño, but cools slightly during July 1998–March 2001, corresponding to a moderate La Niña (Bell et al. 1999, 2000). To investigate changes between these two events, we focus on the differences of SST, OLR, zonal wind stress, surface (10-m) wind speed, surface heating, and dT_s/dt between these two events for the boreal winter of October–March.

a. Changes in SST and atmospheric circulation

To understand the changes in SST and atmospheric circulation over the tropical Pacific and Indian Oceans, the El Niño–La Niña differences in SST, OLR, zonal wind stress, and surface wind speed are shown in Fig. 8 for a large domain of 30°S–30°N, 40°E–120°W. Compared to La Niña, the SST during El Niño increases by ~2°–5°C in the central and eastern equatorial Pacific and by ~1°C in the western equatorial Indian Ocean, but decreases by <1°C near the Maritime Continent

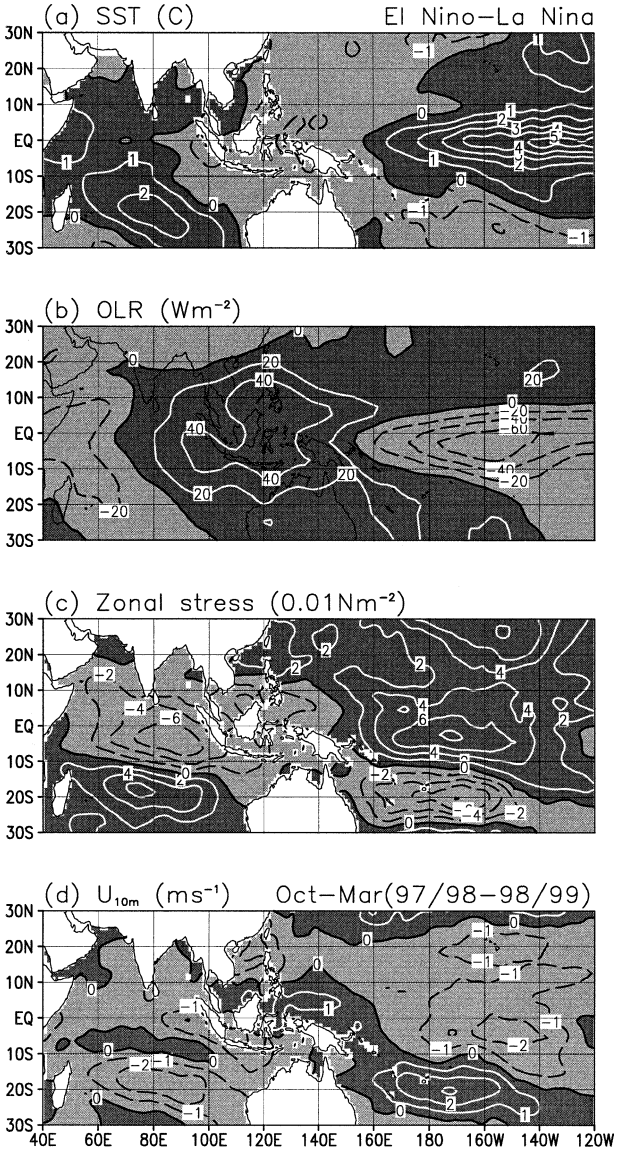

FIG. 8. 1997/98 El Niño − 1998/99 La Niña differences of (a) SST, (b) OLR, (c) zonal wind stress, and (d) 10-m wind speed for the boreal winter Oct–Mar. Positive values are marked with dark shading, and negative values are marked with light shading.

(Fig. 8a). Correspondingly, the OLR decreases by 40–60 and 20 W m^{-2}, respectively, in the central equatorial Pacific and the western equatorial Indian Ocean, but increases by 20–40 W m^{-2} in the Maritime Continent (Fig. 8b). This is an indication of shifting the convection center from the Maritime Continent eastward to the central equatorial Pacific and westward to the western equatorial Indian Ocean.

In the equatorial region during El Niño, the zonal wind stress increases (more westerly as trade winds weaken) east of ~150°E but decreases (more easterly as trade winds strengthen) west of ~150°E (Fig. 8c). In the equatorial region, the changes in OLR and zonal wind stress indicate a weakened Walker circulation in both the Pacific and Indian Oceans during El Niño. During El Niño the zonal wind stress increases in the subtropical regions of the south Indian Ocean and North Pacific, but decreases in the southwestern Pacific near the SPCZ. The latter is due to the northward shift of the SPCZ as indicated by the OLR change. The wind stress change in the southern tropical Indian Ocean is a result of the equatorward shift of trade wind belts during El Niño (Yu and Rienecker 2000). The wind stress change around the South China Sea is an indication of a stronger subtropical high during El Niño, which is consistent with the OLR change there. Compared to La Niña, the surface wind speed generally decreases by ~1–2 m s^{-1} during El Niño except for the regions extending from the southern section of the South China Sea to the Maritime Continent and farther to the SPCZ where cloudiness decreases (Fig. 8d). The El Niño–La Niña difference in the atmospheric circulation in the tropical Indian and Pacific Oceans inferred from the OLR and zonal wind stress (Figs. 8b and 8c) is consistent with the coupled general circulation model (GCM) study of Venzke et al. (2000).

The El Niño–La Niña difference in the zonal wind stress (Fig. 8c) suggests some important interannual variability of ocean dynamics. The stronger easterly zonal wind stress near the equator during El Niño can cause upwelling (downwelling) in the eastern (western) equatorial Indian Ocean. This is related to the Indian Ocean dipole mode and has been extensively discussed in a number of studies (e.g., Webster et al. 1999; Saji et al. 1999; Yu and Rienecker 2000). Furthermore, the stronger easterly zonal wind stress in the equatorial Indian Ocean during El Niño can increase the oceanic heat transport from the south to the north Indian Ocean (e. g., Loschnigg and Webster 2000). The stronger westerly zonal wind stress in the equatorial Pacific during El Niño corresponds to the relaxed trade winds, which not only can push the Pacific warm pool eastward but also can reduce the pressure gradient from the Pacific to the Indian Ocean across Indonesia and, hence, weaken the Indonesian Throughflow for transporting heat from the Pacific to Indian Ocean (e.g., Godfrey 1996; Lukas et al. 1996; Meyers 1996). Finally, it is generally recognized that weakened surface winds can reduce the oceanic mixed layer depth and, hence, enhance the penetration of solar radiation through the mixed layer (e.g., Anderson et al. 1996; Sui et al. 1997; Godfrey et al. 1998; Chou et al. 2000). Therefore, the interannual variability of wind stress is expected to have a significant impact on the mixed layer heat budget and SST variations in this climatically important region through the changes not only in the surface heat fluxes but also in the ocean dynamics.

b. Changes in surface heating and dT_s/dt

The El Niño–La Niña differences in F_{SW}, F_{LH}, F_{NET}, and dT_s/dt for the region 30°S–30°N, 90°E–170°W are

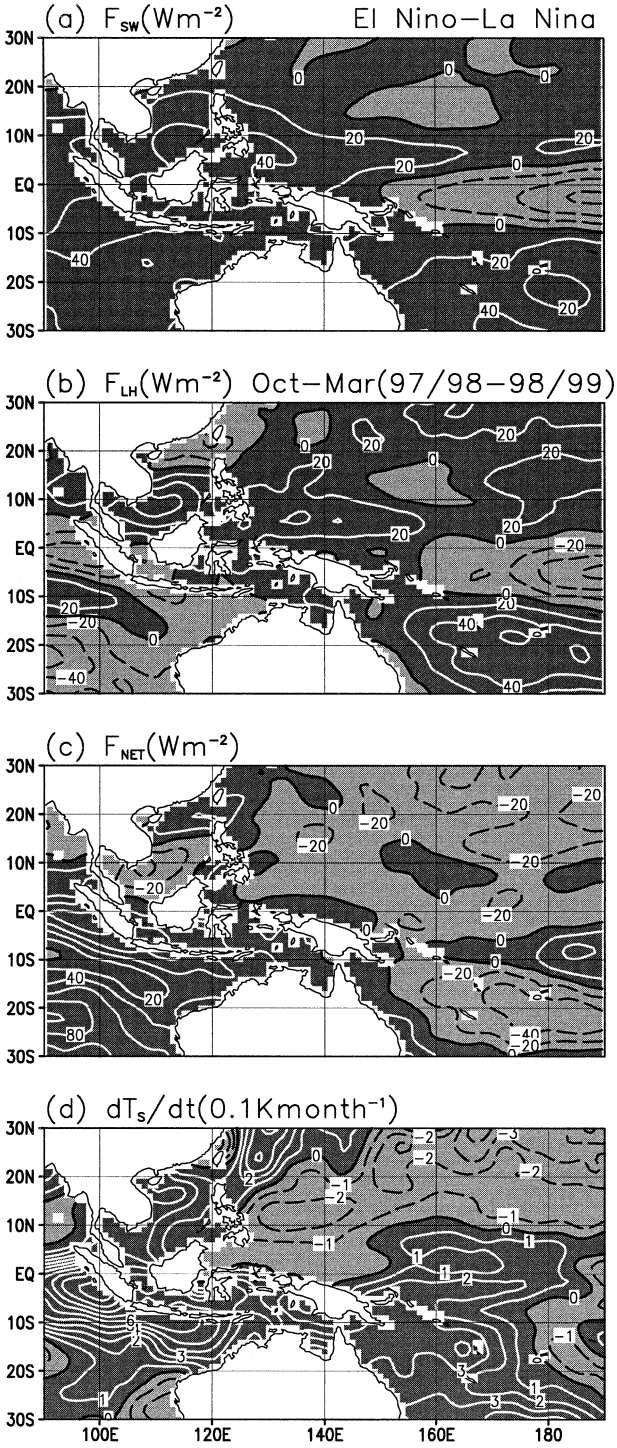

FIG. 9. As in Fig. 8 except for (a) solar heating, (b) evaporative cooling, (c) net surface heating, and (d) SST tendency.

shown in Fig. 9. In accordance with the change in cloudiness, F_{SW} decreases in the equatorial central Pacific but increases in the rest of the domain during El Niño. The pattern of the change of F_{LH} is similar to that of the surface wind. The spatial variation of the F_{LH} change is much greater than that of the F_{SW} change and, hence, dominates the variation of the F_{NET} change. The dominating role of F_{LH} in determining the change of F_{NET} between El Niño and La Niña is demonstrated in Table 4. In the central equatorial Pacific the cloudiness increases but wind decreases during El Niño. Correspondingly, both F_{SW} and F_{LH} decrease with increasing SST. The decrease of F_{LH} surpasses the decrease of F_{SW}, leading to an increase of F_{NET}. So, the enhancement of convection and cloudiness in the central equatorial Pacific associated with a higher SST leads to an enhancement of surface heating with a maximum of 50 W m^{-2} at 8°S, 175°W.

TABLE 4. Differences in the surface heating between the 1997/98 El Niño and 1998/99 La Niña (El Niño minus La Niña). Fluxes are averaged over the boreal winter of Oct–Mar. Respectively, F_{SW}, F_{LH}, and F_{NET} are solar heating, evaporative cooling, and net surface heating. Units are W m^{-2}.

	ΔF_{SW}	ΔF_{LH}	ΔF_{NET}
Central equatorial Pacific (8°S, 175°W)	−15	−51	50
Southern SPCZ (22°S, 175°W)	15	60	−56
Northern SCS (20°N, 120°E)	25	−29	52
Southern SCS (6°N, 110°E)	41	65	−38
Southeastern Indian Ocean (22°S, 92°E)	34	−66	109
Eastern equatorial Indian Ocean (0°, 92°E)	38	−54	95

Over a large area in the Pacific warm pool, the SST is nearly homogeneous between 28° and 30°C. Regions with SST $>$ 30°C are rare. Ramanathan and Collins (1991) hypothesized that, in the Pacific warm pool, increases in thick cirrus clouds in response to an increase in SST had an effect of reducing the solar heating of the ocean and limited the SST to the observed high values. Wallace (1992) reasoned that the homogeneous tropospheric temperature in the Tropics is a result of the efficient heat transport by large-scale circulation. Because of the high sensitivity of evaporation to SST in the warm pool, the sea − air temperature difference is necessarily small, and so is the SST gradient. However, our results (Fig. 9c) show that a large surface heating occurs in the region (centered ~8°S, 160°E–170°W) of increased SST and cloudiness (Figs. 8a and 8b), which are consistent with the results of Liu et al. (1994) and Zhang and McPhaden (1995). The large surface heating at the warmest regions is, of course, not sustainable. When the atmospheric and oceanic circulation returns to a normal situation from El Niño, the convection center shifts from the central equatorial Pacific to the Maritime Continent, the strong trade winds set in, the evaporative cooling enhances, and the SST in the central equatorial Pacific returns to its normal values.

Compared to La Niña, the southern section of the SPCZ during El Niño is less cloudy, more windy, and

drier (greater $Q_s - Q_{10m}$) as the SPCZ shifts northward. The first factor enhances the solar heating, but last two factors enhance the evaporative cooling. The change of evaporative cooling exceeds the change of solar heating, resulting in a larger net surface cooling during El Nino. The region of reduced F_{NET} covers a large area with a maximum of 56 W m^{-2} at 22°S, 175°W.

In the South China Sea (SCS), the change of F_{SW} is positive, but the change of F_{LH} between the northern and southern sections of SCS is in different directions. The change of F_{NET} is large in both the northern and southern sections but with opposite signs, as dominated by F_{LH}. The maximum change of heating in the northern section of the SCS and the maximum change of cooling in the southern section of the SCS are ~52 and 38 W m^{-2}, respectively.

In the eastern Indian Ocean, the F_{NET} change is also dominated by the F_{LH} change. The large increases of F_{NET} in the southeastern Indian Ocean, ~109 W m^{-2}, and in the eastern equatorial Indian Ocean, ~95 W m^{-2}, are due to a large reduction of F_{LH} associated with weakened wind and reduced sea − air humidity difference. The enhanced solar heating due to reduced cloudiness during El Niño (cf. Fig. 8b) also contributes to the large increase of the net surface heating.

It is worth noting that the change of F_{NET} between the 1997/98 El Niño and 1998/99 La Niña is significantly larger in the tropical eastern Indian Ocean than in the tropical western Pacific (Fig. 9c and Table 4). For the eastern Indian Ocean, the reduced evaporative cooling arising from weakened winds during El Niño is generally associated with enhanced solar heating due to reduced cloudiness, leading to a large interannual variability of F_{NET}. For the western Pacific, the reduced evaporative cooling due to weakened winds is generally associated with the reduced solar heating arising from increased cloudiness, and vice versa. Consequently, the interannual variability of F_{NET} is reduced.

The correlation between interannual variations of F_{NET} and dT_s/dt is very weak (Figs. 9c and 9d). In particular, the strong meridional dipolelike change of F_{NET} in the western Pacific south of the equatorial and South China Sea are not consistent with the much smoother change of dT_s/dt. The large net surface heating south of 15°S in the eastern Indian Ocean is also not consistent with the small change of dT_s/dt. Furthermore, the anomalous correlation between the monthly SST tendency and monthly net surface heating computed for the 3-yr period (although it is too short for studying interannual variability) is generally ~0.2–0.5 and is not significant at the 95% level (not shown). These results indicate that the change in ocean dynamics besides the change in surface heating may play an important role in the interannual variation of dT_s/dt. The change in ocean dynamics may include the variations of SW radiation penetrating through the ocean mixed layer, upwelling of cold thermocline water, the Indonesian Throughflow for transporting heat from the Pacific to Indian Ocean, and interhemispheric transport in the Indian Ocean as inferred from the changes in zonal wind stress and surface wind speed (Figs. 8c and 8d). Wang and McPhaden (2001) found that all terms in the heat balance of the oceanic mixed layer contributed to the SST variation in the equatorial Pacific during the 1997/98 El Niño and 1998/99 La Niña. The low correlation between the interannual variations of F_{NET} and dT_s/dt shown in Figs. 9c and 9d is consistent with their finding.

6. Concluding remarks

Seasonal to interannual variations of the net surface heating (F_{NET}) and its relationship to the SST tendency (dT_s/dt) in the tropical eastern Indian and western Pacific Oceans (30°S–30°N, 90°E–170°W) are studied for the 3-yr period October 1997–September 2000. Latent heat flux, sensible heat flux, wind speed, and surface air humidity are derived from the SSM/I radiance measurements, SW and LW fluxes are derived from the Japanese GMS radiance measurements, and SST is taken from the NCEP–NCAR reanalysis.

It is found that the magnitude of solar heating (F_{SW}) is larger than that of evaporative cooling (F_{LH}), but the spatial variation of the latter is significantly larger than the former. The range of the annual mean is 180–240 W m^{-2} for F_{SW} and 80–190 W m^{-2} for F_{LH}. As a result, the spatial variations of seasonal and interannual variability of F_{NET} are dominated by the variability of F_{LH}. Seasonal variations of F_{NET} and dT_s/dt are significantly correlated in the region, except for the equatorial western Pacific. The high correlation is augmented by the high negative correlation between solar heating and evaporative cooling. In the equatorial western Pacific, winds are weak, the oceanic mixed layer is shallow, and the SW radiation penetrating through the mixed layer is significant. Therefore, the relation between F_{NET} and dT_s/dt is weak.

The change of F_{NET} between the 1997/98 El Niño and 1998/99 La Niña is significantly larger in the tropical eastern Indian Ocean than in the tropical western Pacific. For the tropical eastern Indian Ocean, reduced evaporative cooling arising from weakened winds during El Niño is generally associated with enhanced solar heating due to reduced cloudiness, leading to an enhanced interannual variability of F_{NET}. For the tropical western Pacific, reduced evaporative cooling due to weakened winds is generally associated with reduced solar heating arising from increased cloudiness, and vice versa. Consequently, the interannual variability of F_{NET} is reduced. The change in dT_s/dt is generally larger in the tropical eastern Indian Ocean than in the tropical western Pacific. The correlation between interannual variations of F_{NET} and dT_s/dt is very weak for both regions. This result for the equatorial Pacific is consistent with that of Wang and McPhaden (2001) who found that all terms in the heat balance of the oceanic mixed layer contributed to the SST variation in the equatorial Pacific during the

1997/98 El Niño and 1998/99 La Niña. The low correlation is most likely related to the interannual variability of ocean dynamics.

The change in the zonal wind stress suggests some important interannual changes in ocean dynamics. Compared to La Niña, the change of ocean dynamics during El Niño may include an increase of upwelling (downwelling) in the eastern (western) equatorial Indian Ocean and an increase in the interhemispheric heat transport from the south to the north Indian Ocean due to increased easterly wind forcing (Webster et al. 1999; Yu and Rienecker 2000; Loschnigg and Webster 2000). It may also include an increase in heat transport from the equatorial western Pacific to the equatorial central Pacific and a decrease in the heat transport from the Pacific to Indian Ocean by the Indonesian Throughflow due to increased westerly wind focing in the equatorial Pacific (Godfrey 1996; Lukas et al. 1996; Meyers 1996). In addition, the SW radiation penetration through the oceanic mixed layer in the weak wind regions of the equatorial warm pool may change due to the change in surface wind, as suggested by previous studies (e.g., Anderson et al. 1996; Sui et al. 1997; Godfrey et al. 1998; Chou et al. 2000). Thus, we suggest that interannual changes of the surface heating and ocean dynamics all play important roles in the interannual variation of SST in this climatically important region. More observational and modeling studies are needed to validate our conclusions.

The 3-yr mean F_{NET} (40 W m^{-2}) over the western Pacific warm pool is found to be significantly larger than that (7 W m^{-2}) of the TOGA COARE IOP (e.g., Weller and Anderson 1996; Chou et al. 2000). The weak net surface heating during the COARE IOP is due to the much reduced solar heating in the Pacific warm pool associated with unusually high cloudiness. The spatial distributions of surface heat budgets are similar to those of Oberhuber (1988) and Kubota et al. (2002). However, there are quantitative differences, which may be partly due to the difference in time periods of studies and partly due to the differences in the input data and formulas for deriving surface fluxes. In contrast, the 3-yr mean F_{NET} does not agree with those of Gent (1991) and Moisan and Niiler (1998). Gent suggested that the annual-mean net surface heating was 0–20 W m^{-2} in the western Pacific warm pool (10°S–10°N, 140°E–180°). Moisan and Niiler (1998) obtained a surface cooling in the TOGA COARE domain and a weak surface heating confined only to a narrow band west of 140°E in the equatorial region. The results of Gent (1991) and Moisan and Niiler (1998) are significantly smaller than those of Oberhuber (1988), Kubata et al. (2002), and our study.

Acknowledgments. This study was supported by the TRMM Program, Global Modeling and Analysis Program, Radiation Sciences Program, and NASA Office of Earth Science. The SSM/I total precipitable water, wind speed, and antenna temperature were provided by F. Wentz (through the Web site available online at http://www.ssmi.com). The SST and surface air temperature were taken from the NCEP–NCAR reanalysis data archive. Hourly turbulent fluxes measured by research ships were provided by C. Fairall of the NOAA/ETL through the SEAFLUX Web site (online at http://paos.colorado.edu/~curryja/ocean/index.html). The *GMS-5* radiance data used for retrieving surface radiation were provided by the Central Weather Bureau, Taipei, Taiwan. The GSSTF2 turbulent fluxes were obtained online at http://daac.gsfc.nasa.gov/CAMPAIGN_DOCS/hydrology/hd_gsstf2.0.html, and GSSRB radiative fluxes were obtained online at http://daac.gsfc.nasa.gov/CAMPAIGN_DOCS/hydrology/hd_gssrb.html. Valuable suggestions by two anonymous reviewers are highly appreciated.

REFERENCES

Anderson, S. P., R. A. Weller, and R. B. Lukas, 1996: Surface buoyancy forcing and the mixed layer of the western Pacific warm pool: Observations and 1D model results. *J. Climate,* **9,** 3056–3085.

Atlas, R., R. N. Hoffman, S. C. Bloom, J. C. Jusem, and J. Ardizzone, 1996: A multiyear global surface wind velocity dataset using SSM/I wind observations. *Bull. Amer. Meteor. Soc.,* **77,** 869–882.

Bell, G. D., M. S. Halpert, V. E. Kousky, M. E. Gelman, C. F. Ropelewski, A. V. Douglas, and R. S. Schnell, 1999: Climate assessment for 1998. *Bull. Amer. Meteor. Soc.,* **80,** 1040.

——, and Coauthors, 2000: Climate assessment for 1999. *Bull. Amer. Meteor. Soc.,* **81,** 1328.

Chou, M.-D., P.-K. Chan, and M. M.-H. Yan, 2001: A sea surface radiation dataset for climate applications in the tropical western Pacific and South China Sea. *J. Geophys. Res.,* **106,** 7219–7228.

Chou, S.-H., C.-L. Shie, R. M. Atlas, and J. Ardizzone, 1997: Air–sea fluxes retrieved from Special Sensor Microwave Imager data. *J. Geophys. Res.,* **102,** 12 705–12 726.

——, W. Zhao, and M.-D. Chou, 2000: Surface heat budgets and sea surface temperature in the Pacific warm pool during TOGA COARE. *J. Climate,* **13,** 634–649.

——, E. Nelkin, J. Ardizzone, R. M. Atlas, and C.-L. Shie, 2003: Surface turbulent heat and momentum fluxes over global oceans based on the Goddard satellite retrievals, version 2 (GSSTF2). *J. Climate,* **16,** 3256–3273.

Curry, J. A., and Coauthors, 2003: SEAFLUX. *Bull. Amer. Meteor. Soc.,* in press.

da Silva, A., C. C. Young, and S. Levitus, 1994: *Algorithms and Procedures.* Vol. 1, *Atlas of Surface Marine Data 1994,* NOAA Atlas NESDIS 6, 83 pp.

Fairall, C., E. F. Bradley, D. P. Rogers, J. B. Edson, and G. S. Young, 1996: Bulk parameterization of air–sea fluxes for Tropical Ocean Global Atmosphere Coupled Ocean–Atmosphere Response Experiment. *J. Geophys. Res.,* **101** (C2), 3747–3764.

——, ——, J. E. Hare, A. A. Grachev, and J. B. Edson, 2003: Bulk parameterization of air–sea fluxes: Updates and verification for the COARE algorithm. *J. Climate,* **16,** 571–591.

Gent, P. R., 1991: The heat budget of the TOGA-COARE domain in an ocean model. *J. Geophys. Res.,* **96,** 3323–3330.

Godfrey, J. S., 1996: The effect of the Indonesian throughflow on ocean circulation and heat exchange with the atmosphere: A review. *J. Geophys. Res.,* **101,** 12 217–12 237.

——, R. A. House Jr., R. H. Johnson, R. Lukas, J.-L. Redelsperger, A. Sumi, and R. Weller, 1998: Coupled Ocean–Atmosphere Response Experiment (COARE): An interim report. *J. Geophys. Res.,* **103,** 14 395–14 450.

Gruber, A., and J. S. Winston, 1978: Earth–atmosphere radiative heating based on NOAA scanning radiometer measurements. *Bull. Amer. Meteor. Soc.,* **59,** 1570–1573.

Gupta, S. K., N. A. Ritchey, A. C. Wilber, C. H. Whitlock, G. G. Gibson, and P. W. Stackhouse Jr., 1999: A climatology of surface radiation budget derived from satellite data. *J. Climate,* **12,** 2691–2710.

Josey, S. A., E. C. Kent, and P. K. Taylor, 1999: New insights into the ocean heat budget closure problem from analysis of the SOC air–sea flux climatology. *J. Climate,* **12,** 2856–2880.

Kalnay, E., and Coauthors, 1996: The NCEP/NCAR 40-Year Reanalysis Project. *Bull. Amer. Meteor. Soc.,* **77,** 437–471.

Kubota, M., N. Iwasaka, S. Kizu, M. Konda, and K. Kutsuwada, 2002: Japanese Ocean Flux Data Sets with Use of Remote Sensing Observations (J-OFURO). *J. Oceanogr.,* **58,** 213–225.

Lau, K.-M., and P. H. Chan, 1983: Short term climate variability and atmospheric teleconnection from satellite observed outgoing longwave radiation. Part II: Lagged correlations. *J. Atmos. Sci.,* **40,** 2751–2767.

Li, Z., and H. G. Leighton, 1993: Global climatologies of solar radiation budgets at the surface and in the atmosphere from 5 years of ERBE data. *J. Geophys. Res.,* **98,** 4919–4930.

Liu, W. T., J. Zhang, and J. K. B. Bishop, 1994: Evaporation and solar irradiance as regulators of sea surface temperature in annual and interannual changes. *J. Geophys. Res.,* **99,** 12 623–12 637.

Loschnigg, J., and P. Webster, 2000: A coupled ocean–atmosphere system of SST modulation for the Indian Ocean. *J. Climate,* **13,** 3342–3360.

Lukas, R., T. Yamagata, and J. P. McCreary, 1996: Pacific low-latitude western boundary currents and the Indonesian throughflow. *J. Geophys. Res.,* **101,** 12 209–12 216.

Mather, J. H., T. P. Ackerman, W. E. Clements, F. J. Barnes, M. D. Ivey, L. D. Hatfield, and R. M. Reynolds, 1998: An atmospheric radiation and cloud station in the tropical western Pacific. *Bull. Amer. Meteor. Soc.,* **79,** 627–642.

McPhaden, M. J., 1999: Genesis and evolution of the 1997–98 El Niño. *Science,* **283,** 950–954.

Meyers, G., 1996: Variation of Indonesian throughflow and the El Niño–Southern Oscillation. *J. Geophys. Res.,* **101,** 12 255–12 263.

Moisan, J. R., and P. P. Niiler, 1998: The seasonal heat budget of the North Pacific: Net heat flux and heat storage rates (1950–1990). *J. Phys. Oceanogr.,* **28,** 401–421.

Oberhuber, J. M., 1988: An atlas based on the COADS data set: The budgets of heat, buoyancy, and turbulence kinetic energy at the surface of the global ocean. Max Planck Institute for Meteorology Rep. 15, 199 pp.

Palmer, T. N., and D. A. Mansfield, 1984: Response of two atmospheric general circulation models to sea-surface temperature anomalies in the tropical east and west Pacific. *Nature,* **310,** 483–485.

Pinker, R. T., R. Frouin, and Z. Li, 1995: A review of satellite methods to derive surface shortwave radiative fluxes. *Remote Sens. Environ.,* **51,** 108–124.

Ramanathan, V., and W. Collins, 1991: Thermodynamic regulation of ocean warming by cirrus clouds deduced from observations of the 1987 El Niño. *Nature,* **351,** 27–32.

Saji, N. N., B. N. Goswami, P. N. Vinayachandran, and T. Yamagata, 1999: A dipole mode in the tropical Indian Ocean. *Nature,* **401,** 360–363.

Schulz, J., J. Meywerk, S. Ewald, and P. Schluessel, 1997: Evaluation of satellite-derived latent heat fluxes. *J. Climate,* **10,** 2782–2795.

Sui, C.-H., X. Li, K.-M. Lau, and D. Adamac, 1997: Multiscale air–sea interactions during TOGA COARE. *Mon. Wea. Rev.,* **125,** 448–462.

Venzke, S., M. Latif, and A. Villwock, 2000: The coupled GCM ECHO-2. Part II: Indian Ocean response to ENSO. *J. Climate,* **13,** 1371–1383.

Wallace, J. M., 1992: Effect of deep convection on the regulation of tropical sea surface temperature. *Nature,* **357,** 230–231.

Wang, W., and M. J. McPhaden, 2001: Surface layer temperature balance in the equatorial Pacific during the 1997–98 El Niño and 1998–99 La Niña. *J. Climate,* **14,** 3393–3407.

Webster, P. J., T. Palmer, M. Yanai, V. Magana, J. Shukla, R. A. Toma, and A. Yasunari, 1998: Monsoons: Processes, predictability and the prospects for prediction. *J. Geophys. Res.,* **103** (C7), 14 451–14 510.

——, A. Moore, J. Loschnigg, and R. Leben, 1999: Coupled ocean–atmosphere dynamics in the Indian Ocean during 1997–1998. *Nature,* **401,** 356–360.

——, and Coauthors, 2002: The JASMINE pilot study. *Bull. Amer. Meteor. Soc.,* **83,** 1603–1630.

Weller, R. A., and S. P. Anderson, 1996: Surface meteorolgy and air–sea fluxes in the western equatorial Pacific warm pool during the TOGA Coupled Ocean–Atmosphere Response Experiment. *J. Climate,* **9,** 1959–1992.

Wentz, F. J., 1997: A well calibrated ocean algorithm for SSM/I. *J. Geophys. Res.,* **102,** 8703–8718.

Woodruff, S. D., S. J. Lubker, K. Wolter, S. J. Worley, and J. D. Elm, 1993: Comprehensive Ocean–Atmosphere Data Set (COADS) release la: 1980–92. *Earth Syst. Monit.,* **4,** 4–8.

Yu, L., and M. Rienecker, 2000: Indian Ocean warming of 1997–98. *J. Geophys. Res.,* **105,** 16 923–16 939.

Zhang, G. J., and M. J. McPhaden, 1995: The relationship between sea surface temperature and latent heat flux in the equatorial Pacific. *J. Climate,* **8,** 589–605.

Zhang, Y.-C., W. B. Rossow, and A. A. Lacis, 1995: Calculation of surface and top of atmosphere radiative fluxes from physical quantities based on ISCCP data sets. Part 1: Method and sensitivity to input data uncertainties. *J. Geophys. Res.,* **100,** 1149–1165.